NANO LETTERS

pubs.acs.org/NanoLett

Stepwise Nanopore Evolution in One-Dimensional Nanostructures

Jang Wook Choi,[†,⊥] James McDonough,[†,⊥] Sangmoo Jeong,[‡] Jee Soo Yoo,[†] Candace K. Chan,[§,∥] and Yi Cui*[,†]

[†]Department of Materials Science and Engineering, [‡]Department of Electrical Engineering, and [§]Department of Chemistry, Stanford University, Stanford, California 94305

ABSTRACT We report that established simple lithium (Li) ion battery cycles can be used to produce nanopores inside various useful one-dimensional (1D) nanostructures such as zinc oxide, silicon, and silver nanowires. Moreover, porosities of these 1D nanomaterials can be controlled in a stepwise manner by the number of Li-battery cycles. Subsequent pore characterization at the end of each cycle allows us to obtain detailed snapshots of the distinct pore evolution properties in each material due to their different atomic diffusion rates and types of chemical bonds. Also, this stepwise characterization led us to the first observation of pore size increases during cycling, which can be interpreted as a similar phenomenon to Ostwald ripening in analogous nanoparticle cases. Finally, we take advantage of the unique combination of nanoporosity and 1D materials and demonstrate nanoporous silicon nanowires (poSiNWs) as excellent supercapacitor (SC) electrodes in high power operations compared to existing devices with activated carbon.

KEYWORDS Nanopore, nanowire, supercapacitor

Porous materials have been utilized in numerous applications including catalysts,[1,2] molecular sieves,[3] chemical and biological sensors,[4] low k dielectric layers in microelectronic devices,[5] hydrogen storage materials,[6] supercapacitor electrodes,[7] contrast agents for magnetic resonance imaging (MRI),[8] and zeolite-dye microlasers.[9] While template-based syntheses[10,11] have been major methods in producing porous materials with highly ordered pore structures and large surface areas (>1000 m^2/g), the dealloying process has also been utilized to produce a variety of porous materials and expand the materials pool.[12−14] The dealloying process provides unique, complementary advantages to the template-based process; the dealloying process is compatible with various nanomaterials, especially those grown directly on substrates. Therefore, various electrochemical devices whose efficiencies are directly correlated to the yields of surface reactions should benefit substantially from these porous nanostructures. Also, the procedure is simpler because it can be done at room temperature and requires only a couple of reaction steps. Despite these advantages, pore size control in the dealloying methods has been limited to bulk-scale metal alloys focusing on thermal annealing[13] and alloying with additional elements.[15] Hence, it must be meaningful to understand pore evolution in various materials beyond metals and thus develop the capability of controlling the porosities of those materials. In particular, nanopore generation and their size control in nanomaterials should prove to be very useful in diverse applications.

In this study, established Li-battery cycles are used to generate porous, one-dimensional (1D) nanostructures such as porous zinc oxide nanorods (ZnONRs), silicon nanowires (SiNWs), and silver nanowires (AgNWs). We chose these materials because their bonding characteristics are completely different such that the dealloying process is expected to produce nanopores in distinct ways. Because of the small dimensions of the nanowires and nanorods, the pore formation can be observed clearly using electron microscopes. Moreover, the pore evolution can be monitored quantitatively at its various stages of pore growth. Among many potential applications that can take advantage of these well-bound nanostructures with increased surface areas, supercapacitors are demonstrated here as a useful example. Detailed descriptions for nanostructure growth processes, battery sample preparation, and potential profiles for the battery cycles are presented in the Supporting Information (Figures S1 and S2).

In the anode during a Li-battery cycle, Li is inserted during the charging process and is extracted during the discharging process. During the charging process, ZnO goes through the following conversion reaction followed by an alloying reaction

$$2Li + ZnO \leftrightarrow Li_2O + Zn \quad (1)$$

$$Zn + Li \leftrightarrow LiZn \quad (2)$$

Once zinc oxide is lithiated in reaction 1, zinc nanograins are formed in a lithium oxide matrix.[16] If the lithiation

* To whom correspondence should be addressed. E-mail: yicui@stanford.edu.

∥ Present address: Department of Chemistry, University of California, Berkeley, CA 94720.

⊥ These authors contributed equally to this work.

Received for review: 01/23/2010
Published on Web: 03/25/2010

DOI: 10.1021/nl100258p | *Nano Lett.* **2010,** *10,* 1409–1413

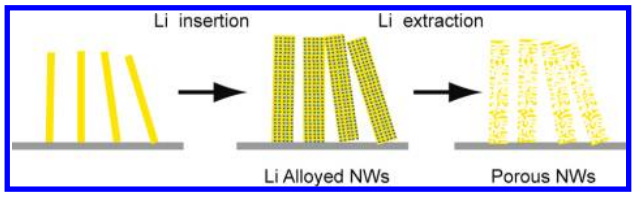

FIGURE 1. Schematic illustration of pore generation by the alloying/dealloying process. As-grown single-crystalline zinc oxide nanorods or silicon nanowires expand upon electrochemical Li ion insertion. As Li ions are extracted from these 1D nanomaterials, the nanostructures shrink but to volumes larger than the original. The increased volumes suggest pore formation inside the nanostructures.

proceeds further, the zinc nanograins become lithiated (reaction 2). The conversion reaction (reaction 1) is confirmed by potential profiles (the plateau at ~0.5 V, Supporting Information Figure S2) consistent with previously reported data[17,18] as well as high resolution transmission electron microscopy (HRTEM) data (Supporting Information Figure S3). On the other hand, Li-battery cycles in silicon are based solely on an alloy-dealloy reaction

$$Si + 4.4Li \leftrightarrow Li_{4.4}Si$$

In the charging process (lithium insertion), the active electrode materials, ZnONRs and SiNWs in our case, undergo volume expansion. Theoretically, ZnO can take 3.0 Li per ZnO, and the volume upon full lithiation is about 163% of the original.[17] Si can take up about 4.4 Li per Si, and its volume upon the full lithiation is even larger, up to 400% of the original. As Li is extracted in the discharging process, the expanded active materials shrink, but the final volume at the end of the discharging is still larger than the original, which indicates formation of void space inside the active materials (Figure 1). Thus, the pore formation depends directly on the volumetric expansion of the active materials in the charging process and the atomic diffusion of the active materials in the discharging process. When the atomic diffusion of active materials is slow during the discharging process, the active materials tend to form pores more efficiently because the slow diffusion prohibits the active materials from returning to their original structures. Instead, thermodynamically metastable structures with pores generated inside are preferred.

Several interesting features in the pore evolution are noteworthy. First, we demonstrate that pore sizes are tunable by the number of Li-battery cycles. As shown in Figure 2, after every Li-battery cycle, pore sizes increase in a stepwise manner for both ZnONRs and SiNWs. The pore size increases are indicated by faster increases of pore volumes compared to those of BET (Brunauer−Emmett−Teller) surface areas (Figure 2B) as well as pore size distributions (Figure 2C). In fact, as the number of Li-battery cycles increase from 5 to 10 cycles, the BET surface areas decreases for both materials. This observation is consistent with the significant pore size increases in the pore size distribution (PSD) data during the same Li-battery cycling period. The stepwise pore size increase can be interpreted as a surface energy reduction brought about by larger pore sizes. Similarly to Ostwald ripening[19] in analogous nanoparticle cases[20] in which nanoparticles are likely to agglomerate in order to minimize surface energy, pores are also likely to increase their widths or merge together to form bigger ones, resulting in a reduction of the surface energy. This is not only the first observation directly related to Ostwald ripening-like phenomena in pore evolution but also provides a clear indication that nanopores can be generated inside diverse 1D nanomaterials and their pore sizes are tunable by the number of electrochemical cycles. A similar method of producing porous metal oxides by using Li-battery cycles has been reported.[21] However, their materials were limited to metal oxides, and adjustable electrochemical parameters to control the porosities were not explored.

Second, pores evolve in different fashions depending on the structural properties of lithiated active materials. While ZnONRs show dramatic increases in pore volumes and BET surface areas after just one Li-battery cycle, SiNWs show gradual increases throughout Li-battery cycling. In the case of ZnONRs, the most feasible mechanism is that a Kirkendall-like effect between the fast-diffusing Zn in the Zn nanograins and the relatively slowly diffusing O^{2-} ions in the Li_2O matrix leads to a nanograin-to-pore transition. Hollow structures in nanoparticles driven by a similar Kirkendall effect between fast-diffusing cobalt ions and slowly diffusing oxide or sulfide have been reported.[22] Our study here is similar to that case. The zinc nanograins function as templates, directing the pore formation. This hypothesis is further supported by the similar size (1−8 nm) between the nanograins and the pore widths and the narrower PSD. On the other hand, in the case of SiNWs, unstable Si dangling bonds surrounding vacancy sites that could appear in the discharging process might preclude efficient pore formation during their initial cycles. However, the poor diffusivities of Si atoms lead to pore formation on the NW surfaces in the early cycles and eventually further penetration toward the core in the later cycles, as indicated by TEM (Figure 3B) and SEM (Figure 4A) images. Therefore, this template-free mechanism results in a gradual increase in pore volume and a broader PSD. We also tested silver nanowires (AgNWs) to see how atomic diffusion affects the pore evolution. Because of the soft nature of silver, pore formation in the nanostructures is not as efficient as in SiNWs and a pore size decrease during 5 to 10 Li-battery cycles was observed, a trend opposite to those of ZnONRs and SiNWs (see Supporting Information Figures S4 and S5 for detailed data and descriptions). Because each porosity data point shown in Figure 2 and Supporting Information S4 is produced from more than 20 Li-battery cells, all of the porosity data should be highly representative.

DOI: 10.1021/nl100258p | *Nano Lett.* **2010,** *10,* 1409--1413

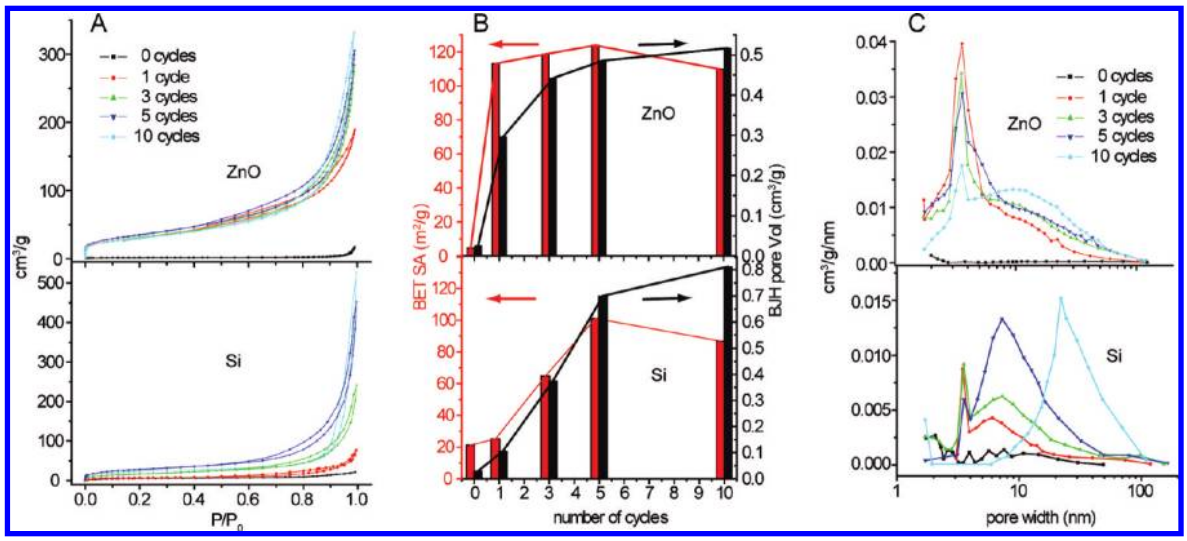

FIGURE 2. Pore size increases with Li-battery cycles. (A) The nitrogen adsorption and desorption isotherms measured at 77 K as a function of the number of Li battery cycles. Increased pore volumes at larger numbers of Li battery cycles are observed for both ZnONRs and SiNWs. (B) The BET surface area and pore volume changes for different numbers of Li-battery cycles. The increase in pore volume is more abrupt than the increase in BET surface area for both materials. Very small pore volumes at 0 Li-battery cycles indicate that interwire spacing is negligible in our measurement range (<300 nm) for both materials. (C) Pore size distributions (PSDs) for different numbers of Li-battery cycles. The pore volume in (B) and the PSD in (C) are obtained from desorption branches using the BJH method.

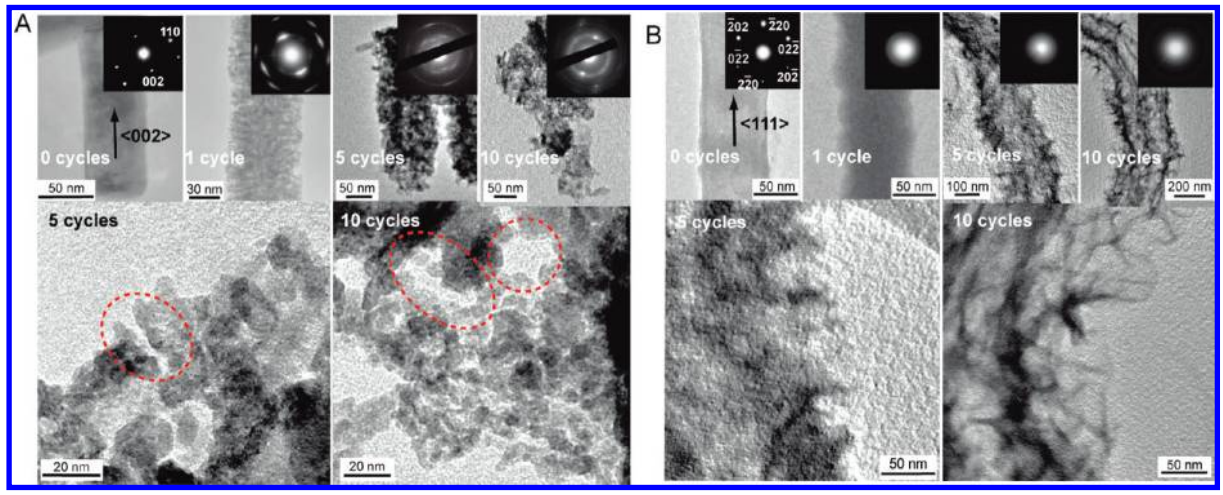

FIGURE 3. TEM images of porous ZnONRs and SiNWs. (A) TEM images for different numbers of Li-battery cycles showing overall morphologies and light/dark contrast in ZnONRs. Light contrast inside the NRs indicates pore formation in the cores of the NRs at larger numbers of Li-battery cycles. Crystal structures indicated by SAED patterns (insets) show a transition from single-crystalline to crystal mosaic to poly crystalline to one close to amorphous as Li-battery cycles go from 0 to 1 to 5 to 10 cycles. In high magnification images, pores formed between grains on the very edges are visible for the ZnONRs at 5 and 10 Li-battery cycles (red dotted circles). These pore widths are consistent with the pore size distribution data in Figure 2C. (B) TEM images of SiNWs for different numbers of Li-battery cycles. During the first cycle, the crystal structure changes from single-crystalline to amorphous, as indicated by SAED patterns (insets). Also, as the number of Li-battery cycles increases, the surface morphologies of SiNWs gets rougher, and light contrast in the middle of NWs increases.

Because pores are formed within the nanomaterials, some pores can be visualized by TEM (Figure 3). Light contrast, indicating void space, is observed in the middle of both nanostructures after 5 and 10 Li-battery cycles. Although 2D imaging by TEM might not be a comprehensive tool for quantitatively analyzing pore sizes for nanopores embedded deep within the 3D structures, pores on the nanostructure edges can be visualized clearly in a high resolution (red dotted circles in HRTEM in Figure 3A). In Figure 3A, the HRTEM image of ZnONRs after 5 Li-battery cycles shows a pore whose width is consistent with the peak around 3.5 nm in the PSD data (Figure 2C). Also, the HRTEM image of ZnONRs after 10 Li-battery cycles shows expanded ink-bottle type pores[23] that again match well with the PSD data in width and distribution. This ink-bottle type pore is not observed in other samples with a smaller number of Li cycles. In addition, crystal structures indicated by selected area electron diffraction (SAED) patterns (insets in Figure 3A,B) also show a clear difference between ZnONRs and SiNWs. ZnONRs show a stepwise transition. Their crystal

DOI: 10.1021/nl100258p | Nano Lett. 2010, 10, 1409–1413

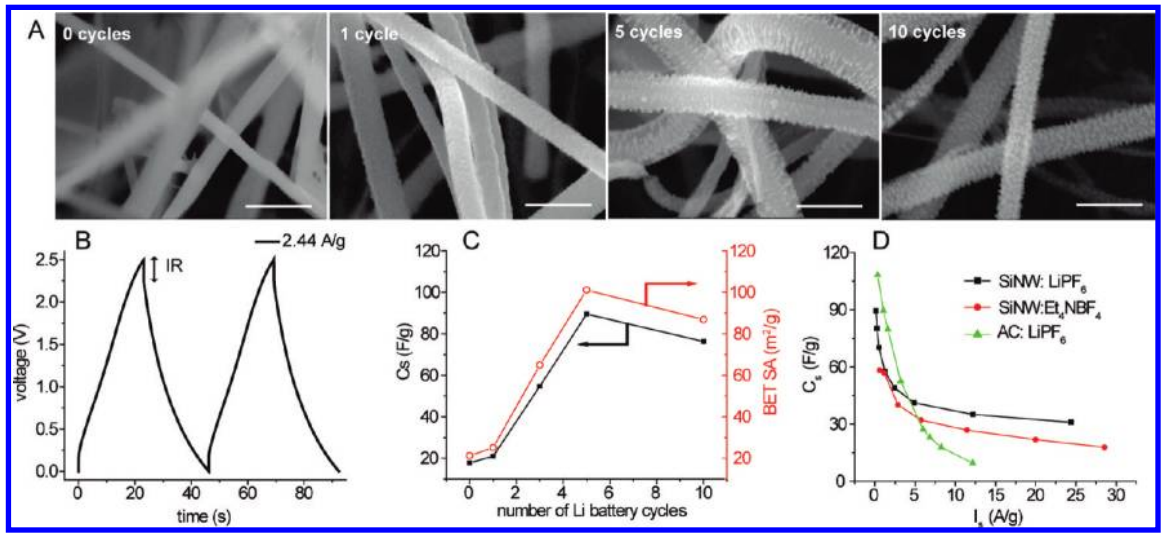

FIGURE 4. Porous SiNWs as supercapacitor electrodes. (A) SEM images of SiNWs after 0, 1, 5, and 10 Li-battery cycles. All the scale bars are 200 nm. (B) A galvanostatic charging/discharging curve taken from a 2.5 V test with $LiPF_6$ in propylene carbonate. The IR drop from the top cutoff potential is also denoted. (C) Gravimetric capacitances and BET surface areas as a function of the number of Li-battery cycles. (D) Gravimetric capacitances for SiNWs after 5 Li-battery cycles and activated carbon are plotted at various charging/discharging currents. Data for SiNWs after 5 Li-battery cycles measured in tetraethylammonium tetrafluoroborate (Et_4NBF_4) are also plotted. The larger capacitances at higher currents suggest that 1D porous nanostructures are more suitable for high power operations than activated carbon, which has much longer, tortuous pore structures and thus inefficient ion diffusion pathways.

structures change from a so-called crystal mosaic (1 cycle) to polycrystalline (5 cycles), then eventually approach an amorphous structure (10 cycles). The crystal mosaic is a transition state between single- and polycrystalline. In this structure, lattice planes in each domain are slightly misaligned with those in the neighboring domains, which result in streaky SAED patterns. In contrast, SiNWs show an abrupt transition such that the crystal structure changes from single-crystalline to an amorphous structure in the first cycle, and the amorphous structure remains persistent in the subsequent cycles (SAEDs in Figure 3B insets). This amorphous character also confirms slow atomic diffusion of Si.

The 1D poSiNWs were tested as supercapacitor (SC) electrodes in order to evaluate how the increased surface areas affect performance. Note that these poSiNWs are intrinsically well-bound to the substrates as a result of the vapor−liquid−solid growth process, a property that should positively affect their performance as SC electrodes. Detailed procedures for cell preparation and data analyses are presented in the Supporting Information. A typical charging/discharging plot during the galvanostatic measurements is presented in Figure 4B. Similar plots were obtained for a series of current values as well as after each Li-battery cycle up to ten cycles. The specific capacitances match well with the BET surface areas over the entire Li-battery cycle range (Figure 4C). Both values increase up to 5 Li-battery cycles then decrease from 5 to 10 Li-battery cycles. The series of current values enables us to see how quickly specific capacitance decreases while the charging/discharging rate increases (Figure 4D). Also, the specific capacitances of poSiNWs are compared with those of activated carbon devices with a similar mass loadings that are the most established among other SC devices. The activated carbon whose capacitance data are plotted in Figure 4D has a BET surface area of ~1070 m^2/g. Nonetheless, its pore structure is completely random, and porous materials of this type only utilize a small fraction of the whole surface area for charge storage. Moreover, their charge storing capabilities become impaired more seriously at higher rates of charging and discharging, which results in specific capacitances that decay very sharply. The superior capacitances of poSiNWs at higher current operations are possible mainly because the organized 1D porous nanostructures are inherently firmly bound to the substrates, eliminating the need for adhesion agents, and allow for far more efficient ion diffusion. For the poSiNWs, the small pore depths, mostly less than tens of nanometers, allows the electrolyte ions to gain access to the electrode surface more efficiently within a given amount of time. Specific capacitances have been measured in different electrolytes as well. The specific capacitances measured from a single device show higher values in lithium hexafluorophosphate ($LiPF_6$) than those in tetraethylammonium tetrafluoroborate (Et_4NBF_4). The electrolyte dependence suggests that electrolyte ions with smaller cross sections exhibit larger specific capacitances when dissolved in the same solvent, propylene carbonate in our case. Although the solvated nature of these electrolyte ions in propylene carbonate may not be completely identical, the specific capacitance trend is reflective of the size effect of the electrolyte ions. The 1D porous nanostructures studied here suggest one of the most ideal structures for SC electrodes. The poSiNW-based SC devices show energy and power densities of ~20 Wh/kg and ~22 kW/kg, respectively, thus exhibiting better

DOI: 10.1021/nl100258p | *Nano Lett.* **2010,** *10,* 1409–1413

performance than most previously reported data (see a Ragone plot in Supporting Information Figure S6).

Various nanomaterials that can be alloyed with Li are expected to hold nanopores in their nanostructures and also exhibit highly tunable porosities by adjusting electrochemical parameters similar to those discussed here. These well-bound porous nanostructures could continue to find many useful applications beyond supercapacitors. For example, porous ZnONRs presented here (~23 times larger surface area compared to nonporous ones might be used as electrodes in dye-sensitized solar cells and yield higher short-circuit currents, currently one of the limiting factors in the area.

Acknowledgment. We thank Brian J. Smith for help in the porosity measurements. J.M. acknowledges support from National Science Foundation and National Defense Science and Engineering Graduate Fellowships. C.K.C. acknowledges support from National Science Foundation and Stanford Graduate Fellowships. This work was partially supported by the King Abdullah University of Science and Technology (KAUST) Investigator Award (No. KUS-l1-001-12) and partially supported by a DOE-EFRC at Stanford: Center on Nanostructuring for Efficient Energy Conversion (CNEEC) (NO. DE-SC0001060).

Supporting Information Available. Experimental procedures, potential profiles of Li-battery cycles, AgNW pore evolution data, and a Ragone plot. This material is available free of charge via the Internet at http://pubs.acs.org.

REFERENCES AND NOTES

(1) Joo, S. H.; Park, J. Y.; Tsung, C. K.; Yamada, Y.; Yang, P. D.; Somorjai, G. A. Thermally stable Pt/mesoporous silica core-shell nanocatalysts for high-temperature reactions. *Nat. Mater.* **2009**, *8*, 126.

(2) Joo, S. H.; Choi, S. J.; Oh, I.; Kwak, J.; Liu, Z.; Terasaki, O.; Ryoo, R. Ordered nanoporous arrays of carbon supporting high dispersions of platinum nanoparticles. *Nature* **2001**, *412*, 169.

(3) Corma, A. From microporous to mesoporous molecular sieve materials and their use in catalysis. *Chem. Rev.* **1997**, *97*, 2373.

(4) Lin, V. S. Y.; Motesharei, K.; Dancil, K. P. S.; Sailor, M. J.; Ghadiri, M. R. A porous silicon-based optical interferometric biosensor. *Science* **1997**, *278*, 840.

(5) Baskaran, S.; Liu, J.; Domansky, K.; Kohler, N.; Li, X. H.; Coyle, C.; Fryxell, G. E.; Thevuthasan, S.; Williford, R. E. Low dielectric constant mesoporous silica films through molecularly templated synthesis. *Adv. Mater.* **2000**, *12*, 291.

(6) Rosi, N. L.; Eckert, J.; Eddaoudi, M.; Vodak, D. T.; Kim, J.; O'Keeffe, M.; Yaghi, O. M. Hydrogen storage in microporous metal-organic frameworks. *Science* **2003**, *300*, 1127.

(7) Pandolfo, A. G.; Hollenkamp, A. F. Carbon properties and their role in supercapacitors. *J. Power Source* **2006**, *157*, 11.

(8) Platas-Iglesias, C.; Vander Elst, L.; Zhou, W. Z.; Muller, R. N.; Geraldes, C.; Maschmeyer, T.; Peters, J. A. Zeolite GdNaY nanoparticles with very high relaxivity for application as contrast agents in magnetic resonance imaging. *Chem.—Eur. J.* **2002**, *8*, 5121.

(9) Vietze, U.; Krauss, O.; Laeri, F.; Ihlein, G.; Schuth, F.; Limburg, B.; Abraham, M. Zeolite-dye microlasers. *Phys. Rev. Lett.* **1998**, *81*, 4628.

(10) Davis, M. E. Ordered porous materials for emerging applications. *Nature* **2002**, *417*, 813.

(11) Yang, P. D.; Zhao, D. Y.; Margolese, D. I.; Chmelka, B. F.; Stucky, G. D. Generalized syntheses of large-pore mesoporous metal oxides with semicrystalline frameworks. *Nature* **1998**, *396*, 152.

(12) Erlebacher, J.; Aziz, M. J.; Karma, A.; Dimitrov, N.; Sieradzki, K. Evolution of nanoporosity in dealloying. *Nature* **2001**, *410*, 450.

(13) Erlebacher, J.; Seshadri, R. Hard Materials with Tunable Porosity. *MRS Bull.* **2009**, *34*, 561.

(14) Weissmuller, J.; Newman, R. C.; Jin, H. J.; Hodge, A. M.; Kysar, J. W. Nanoporous Metals by Alloy Corrosion: Formation and Mechanical Properties. *MRS Bull.* **2009**, *34*, 577.

(15) Snyder, J.; Asanithi, P.; Dalton, A. B.; Erlebacher, J. Stabilized Nanoporous Metals by Dealloying Ternary Alloy Precursors. *Adv. Mater.* **2008**, *20*, 4883.

(16) Poizot, P.; Laruelle, S.; Grugeon, S.; Dupont, L.; Tarascon, J. M. Nano-sized transition-metaloxides as negative-electrode materials for lithium-ion batteries. *Nature* **2000**, *407*, 496.

(17) Wang, H. B.; Pan, Q. M.; Cheng, Y. X.; Zhao, J. W.; Yin, G. P. Evaluation of ZnO nanorod arrays with dandelion-like morphology as negative electrodes for lithium-ion batteries. *Electrochim. Acta* **2009**, *54*, 2851.

(18) Zhang, C. Q.; Tu, J. P.; Yuan, Y. F.; Huang, X. H.; Chen, X. T.; Mao, F. Electrochemical performances of Ni-coated ZnO as an anode material for lithium-ion batteries. *J. Electrochem. Soc.* **2007**, *154*, A65.

(19) Zott, R. Friedrich Wilhelm Ostwald (1853—1932), now 150 years young. *Angew. Chem., Int. Ed.* **2003**, *42*, 3990.

(20) Peng, Z. A.; Peng, X. G. Mechanisms of the shape evolution of CdSe nanocrystals. *J. Am. Chem. Soc.* **2001**, *123*, 1389.

(21) Hu, Y. S.; Guo, Y. G.; Sigle, W.; Hore, S.; Balaya, P.; Maier, J. Electrochemical lithiation synthesis of nanoporous materials with superior catalytic and capacitive activity. *Nat. Mater.* **2006**, *5*, 713.

(22) Yin, Y. D.; Rioux, R. M.; Erdonmez, C. K.; Hughes, S.; Somorjai, G. A.; Alivisatos, A. P. Formation of hollow nanocrystals through the nanoscale Kirkendall Effect. *Science* **2004**, *304*, 711.

(23) Lowell, S.; Shields, J. E.; Thomas, M. A.; Thommes, M. *Characterization of Porous Solids and Powders: Surface Area, Pore Size and Density*; Springer: New York, 2006.

DOI: 10.1021/nl100258p | *Nano Lett.* **2010,** *10,* 1409--1413